Direct Evidence for Hydrogen Bonding in Glycans: A Combined NMR and Molecular Dynamics Study

ARTICLE *in* THE JOURNAL OF PHYSICAL CHEMISTRY B · MARCH 2013

Impact Factor: 3.3 · DOI: 10.1021/jp400402b · Source: PubMed

4 AUTHORS, INCLUDING:

Robert Pendrill
Stockholm University
17 PUBLICATIONS **100** CITATIONS
SEE PROFILE

Darón I Freedberg
U.S. Food and Drug Administration
52 PUBLICATIONS **1,588** CITATIONS
SEE PROFILE

THE JOURNAL OF PHYSICAL CHEMISTRY B

Article

pubs.acs.org/JPCB

Direct Evidence for Hydrogen Bonding in Glycans: A Combined NMR and Molecular Dynamics Study

Marcos D. Battistel,[†] Robert Pendrill,[‡] Göran Widmalm,[‡] and Darón I. Freedberg*[,†]

[†]Laboratory of Bacterial Polysaccharides, Center for Biologics Evaluation and Research, Food and Drug Administration, 1401 Rockville Pike, Rockville, Maryland 20852-1448, United States

[‡]Department of Organic Chemistry, Arrhenius Laboratory, Stockholm University, S-106 91 Stockholm, Sweden

Supporting Information

ABSTRACT: We introduce the abundant hydroxyl groups of glycans as NMR handles and structural probes to expand the repertoire of tools for structure−function studies on glycans in solution. To this end, we present the facile detection and assignment of hydroxyl groups in a wide range of sample concentrations (0.5−1700 mM) and temperatures, ranging from −5 to 25 °C. We then exploit this information to directly detect hydrogen bonds, well-known for their importance in molecular structural determination through NMR. Via HSQC-TOCSY, we were able to determine the directionality of these hydrogen bonds in sucrose. Furthermore, by means of molecular dynamics simulations in conjunction with NMR, we establish that one out of the three detected hydrogen bonds arises from intermolecular interactions. This finding may shed light on glycan−glycan interactions and glycan recognition by proteins.

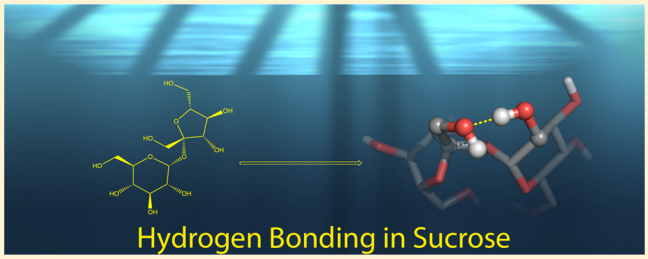

INTRODUCTION

Glycans are of great importance in biological systems. Cells display an enormous diversity of glycans attached to either proteins[1] or lipids[2] that can serve as camouflage or mask antigenic sites.[3] This is often observed for Gram-negative pathogenic bacteria like *Neisseria meningitidis*.[4] Glycans are also important signaling systems, mediators of cell−cell interactions, including self−self[5] and self−pathogen interactions,[6,7] and participate in protein quality control systems.[8,9] The National Academy of Sciences recently issued a roadmap for transforming glycoscience due to glycans' central role in biology, their impact in medicine, energy generation, and material sciences.[10] Carbohydrates' diversity in function can only be accomplished with their vast potential of chemical variation: glycans can be found in two ring sizes (pyranose and furanose), and in open form;[11] two possible configurations of the hydroxyl group at the anomeric carbon (α and β); the potential of polymerization or branching at each hydroxyl group site and the potential chemical modification of hydroxyl groups (sulfates, phosphates, methoxy, carboxyl, and amino groups). This diversity in structure and function in conjunction with their internal motion[12] contributes to glycan complexity, and constitutes a bottleneck for significant scientific progress to relate carbohydrate structure to function. Thus, we direct our efforts toward simplifying the apparent overwhelming complexity by finding structural patterns in carbohydrates, like secondary structures in nucleic acids and proteins. However, structure determination of carbohydrates can be a daunting task.

NMR solution structure determination is a multistep process (Chart 1). The use of isotopic labeling together with multidimensional NMR experiments is mandatory in proteins and nucleic acids. Subsequently, with the goal of resonance

Chart 1. General NMR Structure Determination Guidelines

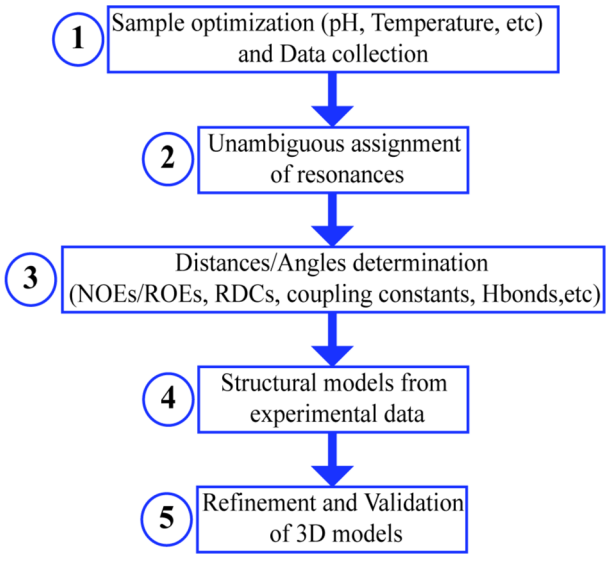

Received: January 13, 2013
Revised: March 24, 2013
Published: March 26, 2013

assignments (step 2, Chart 1), NMR spectroscopists exploit resonance "handles" specific to the biomolecule in question. These handles (imino NHs in nucleic acids and amide NHs in proteins) are well-resolved resonances, partly due to hydrogen bonding, which enable the discrimination of each monomeric unit of the biopolymer. Complete unambiguous assignment (step 2) is desired to interpret the data obtained in step 3. Glycan structural determination has a bottleneck in these two crucial steps of Chart 1. First, unambiguous resonance assignment is not trivial due to signal overlap. Therefore, current handles for resonance assignment (anomeric ^{1}H chemical shifts) are insufficient, or lacking. Second, isotopic enrichment is seldom available, and thus, multidimensional experiments are limited. Third, even when signals are resolved, structural constraints are sparse, partly due to carbohydrate intrinsic flexibility. Steps 2 and 3 (Chart 1) are mandatory for complete structural determination. The work presented in this report is aimed at catalyzing the structural determination of glycans by exploiting exchangeable hydrogen atoms to identify hydrogen bonds (Hbonds) and utilize them as structural constraints. We showed in a recent report[13] that the α2−8-linked sialic acid tetramer can form a helical structure containing three intramolecular hydrogen bonds. Thus, obtaining direct evidence of Hbonds provides invaluable data for uncovering structural patterns in glycans. Moreover, we seek to exploit OH groups, in combination with CH groups, as potential handles for glycan structural studies. Our groups and others[13−19] hold that an enormous wealth of structural information is stored in exchangeable protons such as amide protons (HNs) and hydroxyl protons (OHs). These signals often go undetected because the majority of glycan NMR studies are performed using D_2O as solvent. The groups of van Halbeek, O'Leary, Harvey, and Köver pioneered the observation and exploitation of OH signals in glycans.[15−18,20] However, they resorted to extremely low temperatures 255 K), high sample concentrations (1.4−1.7 M), and mixed or aprotic solvents.[19,21,22] In this combined NMR and molecular dynamics (MD) simulations study, we report the NMR observation of OHs in the disaccharides sucrose and trehalose in natural ^{13}C isotopic abundance. We demonstrate that OHs can be easily assigned in deionized H_2O (pH 6.5) over a wide range of temperatures (263−298 K) and carbohydrate concentrations (50−1200 mM). We then utilize OH resonances as probes to detect Hbonds for sucrose in solution and show that Hbond donor and acceptor can be easily determined, thus establishing Hbond directionality. Additionally, we demonstrate the discrimination between inter- and intramolecular Hbonds through a combination of MD simulations and NMR experiments.

MATERIALS AND METHODS

Sucrose and trehalose samples were prepared at various concentrations (0.5−800 mM) from serial dilutions of stock solutions of 1.6 and 1.2 M containing 10% D_2O, 0.05% NaN_3, and 0.1% DSS as internal reference for chemical shift and internal temperature determination. pH was adjusted to 6.5 (uncorrected for isotope effect) which was found to be optimal for sucrose and trehalose hydroxyl group observation and assignment.

All NMR experiments were performed either on a Bruker Avance 700 MHz spectrometer equipped with an *xyz*-gradient QXI room temperature probe or on a Bruker Avance III 500 MHz spectrometer equipped with a *z*-gradient QXI probe.

NMR data were processed using nmrPipe and analyzed with nmrDraw,[23] TopSpin 2.0, or CCPNMR analysis software.[24]

NMR Experiments. *Hydroxyl Protons.* Hydroxyl proton resonances were observed in one-dimensional (1D) proton experiments with 3-9-19 WATERGATE module for water suppression[25] (Bruker pulse sequence p3919gp) over a wide range of sucrose concentrations (0.5−1700 mM) and temperatures (268−283 K); however, unambiguous assignment was carried out in sucrose samples in water at concentrations higher than 50 mM to proportionally decrease experimental time. The carrier frequency, spectral window (SW), number of scans, number of points, and recycle delay were set to 4.7 ppm, 16 ppm, 32, 8192, and 1.5 s, respectively. One-dimensional experiments were processed without apodization.

Sample Optimization. Sucrose samples in deionized water were prepared at a concentration of 100 mM and the pH was adjusted to 5, 5.5, 6, 6.5, 7, and 7.5 with NaOH or HCl. 1D ^{1}H spectra were collected at 268 K. Spectra from samples at pH 6.5 yielded maximum hydroxyl proton signals. Consequently, phosphate buffer (pH 6.5) samples of different concentrations were prepared (0, 20, 50, 100, and 150 mM). We found that deionized water, as opposed to dilute buffer, favored OH detection.

Because pH is temperature dependent, we measured pH over a wide range of temperatures and sample concentrations. We utilized the same samples as for the NMR experiments. To determine sample pH outside the magnet, a JASCO PDF-425S unit was used to control sample temperature in the 263−298 K range. NMR samples were transferred to Eppendorf tubes and pH was measured at 298 K. Subsequently, the sample was equilibrated for 10 min at the target temperature (263, 268, 273, and 278 K), then pH was measured. Each measurement was done in triplicate. The same procedure was repeated for sucrose at 200, 300, and 800 mM. The pH for 300 mM or more diluted samples could not be determined below 268 K as the samples froze in the Eppendorf tube (however, they did not freeze in a Wilmad tube, at the same temperature). The pH values did not vary significantly for the range of temperatures and concentrations tested. The average pH (±standard deviation, SD) for all the samples at different temperatures yielded pH = 6.58 ± 0.10, Figure S1 in the Supporting Information).

Assignments. Two-dimensional (2D) HSQC-TOCSY experiments[26] (Bruker pulse sequence hsqcdietf3gpsi) were used to assign hydroxyl groups. A 10 ms total DIPSI spinlock mixing time (τ_m) was utilized to ensure that only correlations between the hydroxyl group and geminal protons were observed. The WALTZ17 ^{13}C decoupling sequence was selected as it produced less sample heating and decoupling sideband artifacts compared to GARP, GARP4, WALTZ16, and MLEV16.

The carrier frequencies, SW, number of points, and recycle delay were set to 4.75 and 68 ppm; 5 and 20 ppm; 4096, 128, and 1.8 s, for ^{1}H and ^{13}C, respectively. HSQC-TOCSY data, for hydroxyl signal assignment and Hbond detection, were processed with nmrPipe applying Lorentz-to-Gauss (g1 = 10, g2 = 10) and a cosine bell apodization in the direct and indirect dimensions, respectively.

For a 100 mM sucrose sample at 268 K, 64 scans and 64 t_1 points (2 h experimental time) were sufficient to produce good quality data for unambiguous assignment of hydroxyl protons. The resulting signal/noise was greater than 20/1 on a 500 MHz Bruker Avance III instrument.

dx.doi.org/10.1021/jp400402b | J. Phys. Chem. B 2013, 117, 4860−4869

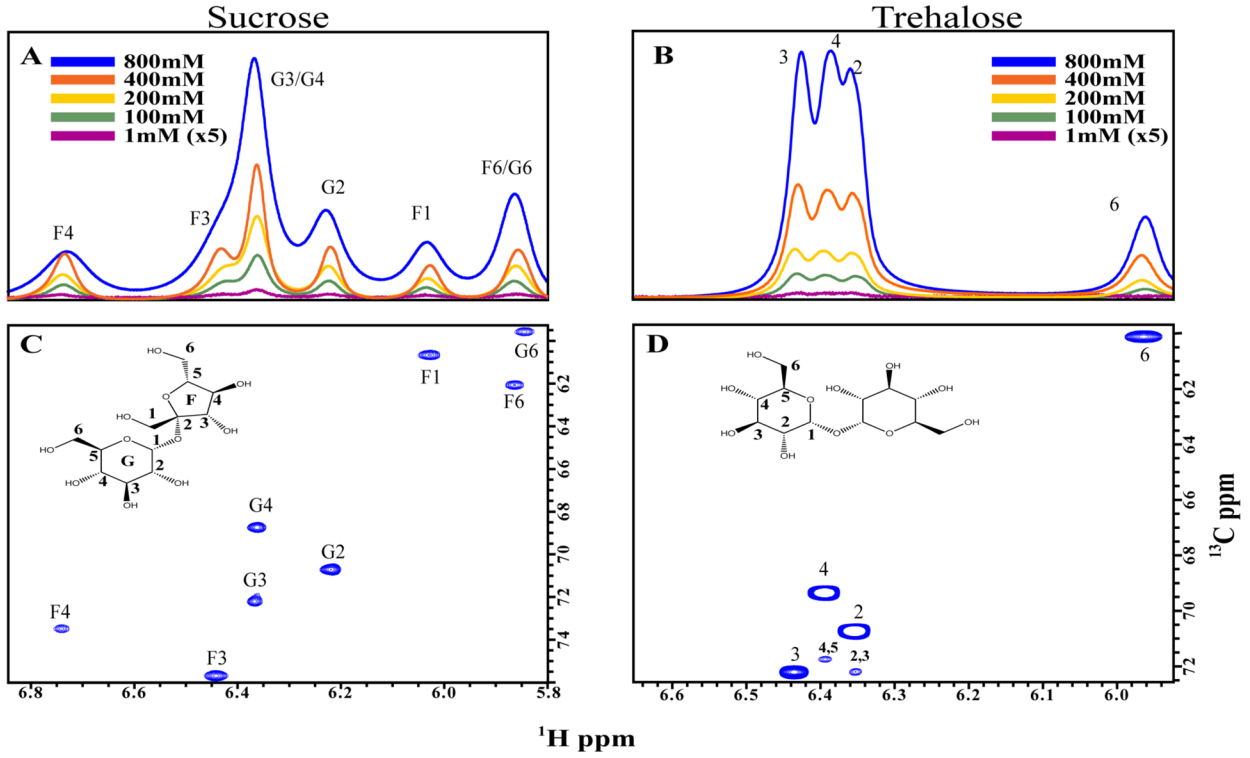

Figure 1. Series of 1H 1D spectra at various sucrose (panel A) and trehalose (panel B) concentrations, collected at 268 K, pH 6.5. Hydroxyl proton regions of 2D ^{1}H,^{13}C HSQC-TOCSY spectra, tuned for hydroxyl proton detection for sucrose and trehalose (panels C and D, respectively). Atom assignments for sucrose are indicated with letters G (glucose ring) and F (fructose ring) followed by arabic numerals to indicate atom position. For trehalose (D) atom assignments are indicated only with arabic numerals because atoms belonging to different residues are indistinguishable due to symmetry.

Hydrogen Bonds via NMR Detection. Hydrogen bond detection and Hbond donor and acceptor determinations (directionality) were carried out utilizing the same SWs and carrier frequencies as for hydroxyl proton detection. However, the τ_m and t_1 points were increased to 30 ms and 128, respectively, with respect to previous experiments. In a 200 mM sucrose sample (minimum concentration at which Hbonds were detected) where 256 scans were required to observe Hbonds, the signal/noise ratio of the cross peaks was greater than 10/1, totaling 18 h of data collection.

Control Experiment: Selective COSY. Square nonselective pulses in the Bruker pulse sequence COSYgpqf[27] were replaced by selective Eburp (7.8 ms), phase-modulated 90° pulses, before and after the t_1 evolution. Additionally, a 2 ms selective half-Gaussian water flip-back pulse was incorporated at the end of the pulse sequence. These pulses were utilized to excite resonances at both sides of the water without perturbing the water magnetization, and thus maximized water suppression. 512 scans were accumulated for each of the 128 t_1 increments. A SW of 10 ppm was used in both ^{1}H dimensions with the carrier frequency set at 4.68 ppm. A recycle delay of 1.5 s was used. Sine-bell functions were applied to both proton dimensions for processing.

Sucrose Concentration Dependence Studies. The data collected for different carbohydrate samples were processed with nmrPipe software.[23] Hbond peak volumes and intensities were calculated using the nmrPipe fitting program fitTab.tcl.

Translational Diffusion. Translational diffusion data were collected utilizing the Bruker pulse sequence stedpgp1s19pr.[28,29] Diffusion constants were obtained using TopSpin 2.0 diffusion analysis module, by fitting the curves resulting from plotting peak intensity at different gradient strengths, following the procedure described by Windig and Antalek.[30]

Molecular Dynamics. Molecular dynamics (MD) simulations were performed using CHARMM[31] (parallel version, C36b1) together with the CHARMM2010[32] force field. Langevin dynamics simulations were performed at a temperature of 310 K with the collision frequency set to 50 ps^{-1} for all heavy atoms[33] and a value of 3 for the dielectric constant. For restrained MD simulations, a harmonic restraint was applied to the distance between the F3 oxygen atom and the G3 or G4 oxygen atom, respectively, with the force constant set to 10 kcal mol^{-1} Å^{-2} and the target distance equal to 3.2 Å. The potential energy of the system after applying the restraint was minimized using steepest descent, 1000 steps, prior to the Langevin dynamics simulation which was integrated using a 1 fs time step until a trajectory of 1 μs had been collected, saving the coordinates every 1000 steps.

For MD simulations studying the intermolecular hydrogen bond concentration dependence, geometries for small crystals having 2, 4, 8, 10, 12, 14, 16, 18, and 20 sucrose molecules were generated from neutron diffraction data.[34] These were placed in a previously equilibrated cubic water box having sides of 29.972 Å, each containing 900 TIP3P water molecules.[35] Water molecules closer than 2.4 Å to the solutes were removed, leaving 871, 839, 777, 749, 725, 702, 666, 648, and 624 solvent molecules for the different crystal sizes, respectively. The potential energies of these systems were minimized using steepest descent, 100 steps, followed by adopted basis Newton−Raphson, 5000 steps or until the rms gradient was less than 0.01 kcal mol^{-1} Å^{-1}, before assigning velocities at 100

dx.doi.org/10.1021/jp400402b | J. Phys. Chem. B 2013, 117, 4860−4869

K and heating to 283 K during 40 ps. Production runs were performed for 50 ns using periodic boundary conditions with an NPT ensemble, using the Langevin piston algorithm[36] to maintain constant pressure (1 atm) and temperature. Nonbonded forces were switched to zero between 10 and 12 Å, using the particle mesh Ewald approach for electrostatics. Bonds to hydrogen atoms were restrained using SHAKE and a time step of 2 fs was used, saving coordinates every 2 ps. The initial parts of the trajectories were treated as equilibration and not used for analysis. The length of the equilibration period needed for homogeneous dissolution to occur was determined by using time-resolved sugar−sugar radial distribution functions to be from 2 ns for the smallest up to 6 ns for the largest crystal sizes, respectively. The MD simulations were carried out on one node with 8 cores using a Dell Harpertown Foundation Level System (FLS) cluster at the Center for Parallel Computers, KTH, Stockholm, Sweden.

RESULTS AND DISCUSSION

To use exchangeable ^{1}H signals as structural probes, we optimized their detection (first step in Chart 1) using sucrose and trehalose as model systems. Figure 1A,B shows ^{1}H NMR spectra of sucrose and trehalose in H_2O, at various concentrations. The spectra clearly show that OH groups can be observed in 1D experiments and even at low concentrations. To assign these peaks, we sought to obtain the sharpest possible lines to yield the best signal-to-noise ratios. We found that the OH signals' line widths can be optimized by fine-tuning pH and salt concentration. Adjusting pH to 6.5 and using HPLC-grade, deionized water, yielded narrow (∼15 Hz) and more intense peaks; whereas, as little as 20 mM phosphate (pH 6.5) roughly halved signal intensity and increased line widths by 2-fold (data not shown). Temperature and sample concentration are important parameters for OH detection. Lower temperatures and higher sample concentration decrease hydroxyl proton exchange with the solvent and, thus, favor their detection. As expected, increasing sucrose concentration from 400 to 800 mM results in a 2-fold increase in signal/noise; however, line width also increases. The latter diminishes signal resolution (note that F3, G3, and G4 signals overlap at 800 mM) in 1D spectra. Additionally, NMR experiments for sucrose and trehalose samples exceeding 1.2 M, at or below 273 K, further increases sample viscosity,[37] resulting in significant signal loss (Figure S2 in the Supporting Information), probably due to slow molecular tumbling.

1D ^{1}H signals for G6, F6 and G3, G4 in sucrose are overlapped; therefore, they cannot be assigned without increasing resolution with a second NMR dimension (Figure 1A). To assign these peaks, we utilized the 2D HSQC-TOCSY experiment[26] (Figure 1C, and Table S1 in the Supporting Information). Using the ^{13}C resolution inherent in this experiment, we assigned the hydroxyl ^{1}Hs for sucrose and trehalose. Our assignments agree with previous reports on sucrose[17] and trehalose.[38] The efficiency of a TOCSY transfer[39] between an OH and its geminal ^{1}H is essential for assigning the exchangeable hydroxyl ^{1}Hs. Panels C and D of Figure 1 show that, with this experiment, each OH group in sucrose and trehalose can be unambiguously correlated to its corresponding carbon (via a geminal ^{1}H to the hydroxyl group). For an 800 mM sucrose sample (700 MHz, 268 K), we collected data for OH signals assignment in less than 2 h, obtaining cross peaks with S/N values of at least 80/1. If one desires to reduce experimental time even further, one alternative is to utilize a narrower spectral window in the indirect dimension (3 ppm) and carefully optimize for signal aliasing (Figure S3 in Supporting Information). Employing this strategy, experimental time can be reduced ca. 17-fold, because fewer t_1 points are required to achieve the same resolution as for an experiment of a larger spectral window in ^{13}C. Another alternative is to use ^{13}C-labeled compounds, which would decrease the experimental time and sample concentrations requirement to perform OH assignment experiments, but would require constant time in the ^{13}C dimension.

A TOCSY mixing time of 10 ms is ideal for OH assignment because OH signals correlate to ^{13}C through geminal ^{1}Hs. Henceforth, we call these types of correlations autocorrelations, because the cross peaks observed link a hydroxyl signal to its proximate ^{13}C.

Free from water signal interference, the hydroxyl signal region (∼5.4−7 ppm) provides additional signal dispersion that can be exploited for resonance assignment. Additionally, they may resolve ambiguities when correlation peaks between directly attached protons and carbons overlap. Detection and assignment of OH groups are the first steps for their utilization as resonance handles in carbohydrates.

Longer τ_m values lead to additional TOCSY cross peaks that, in the absence of assignments, may be misinterpreted as autocorrelation peaks. These types of peaks are shown in the HSQC-TOCSY spectrum of trehalose (Figure 1D) (labeled 4,5 and 2,3); however, in this case, they are easily distinguished from autocorrelations by their lower intensities. Discrimination of auto versus long-range correlation signals becomes more difficult at longer τ_m. Therefore, we recommend using short τ_m values for correctly assigning hydroxyl groups.

We next explored the OH peaks' temperature dependence behavior in sucrose (Figure 2A). As expected, we observed a significant decrease of peak intensity with concomitant broadening (from ∼15 Hz at 268 K to ∼65 Hz at 283 K) at higher temperatures, which is likely due to exchange broadening (Figure 2A). At 700 MHz, sucrose OH signals can be assigned up to 283 K (Figure 2A), whereas trehalose OH signals were assignable up to 298 K (Figure 2B). Naturally, increasing the number of scans and experiment resolution in the ^{13}C dimension will yield higher S/N. Furthermore, utilizing higher magnetic fields will certainly extend the temperature and sample concentration observable range of hydroxyl groups by providing more sensitivity and a larger resonance frequency difference with respect to the water resonance.

Previous studies of glycan hydroxyl groups focused on decreasing hydroxyl ^{1}H exchange with the solvent to permit their identification via homonuclear experiments. This was accomplished by increasing sample concentration,[15,18] by lowering the temperature,[17] and in numerous cases by using mixed or aprotic solvents.[15,19,21,22,40−42] The first two strategies enabled ^{1}Hs resonance assignment and even coupling constant measurements. However, high sample concentration and using mixed solvents are not desirable because these conditions may favor conformations not present in dilute water solution; therefore, the obtained data may not be relevant to glycan structure under physiological conditions.[42] Alternatively, working under supercooled conditions (255 K[17]) is a better approach, because it favors the observation of more stable conformations already present in solution. However, one seeks to perform structural studies at, or closer to, physiological conditions because it affords a more relevant interpretation of structure−function relationships in a biological context. The

dx.doi.org/10.1021/jp400402b | J. Phys. Chem. B 2013, 117, 4860−4869

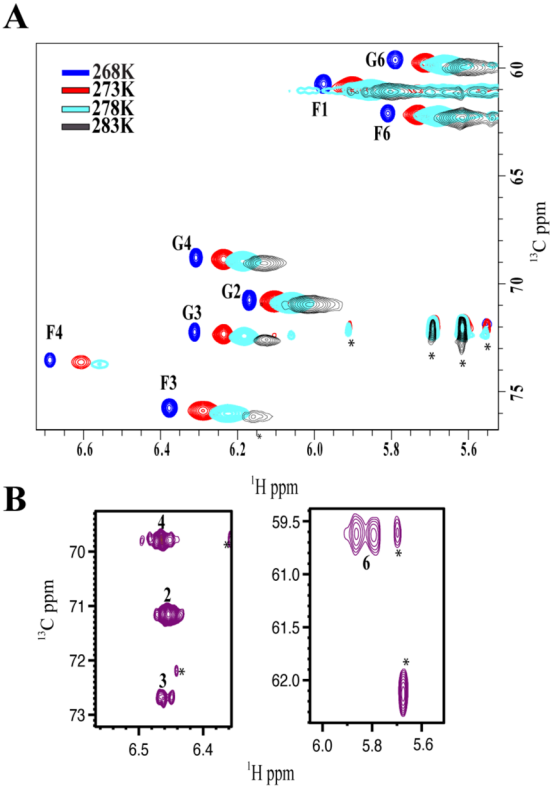

Figure 2. (A) OH region of an HSQC-TOCSY spectra for 800 mM sucrose (pH 6.5) in deionized H_2O at different temperatures, collected at 700 MHz. Asterisks indicate ^{13}C decoupling artifacts. (B) OH regions of HSQC-TOCSY spectrum of an 800 mM trehalose sample at 298 K; asterisks denote impurities.

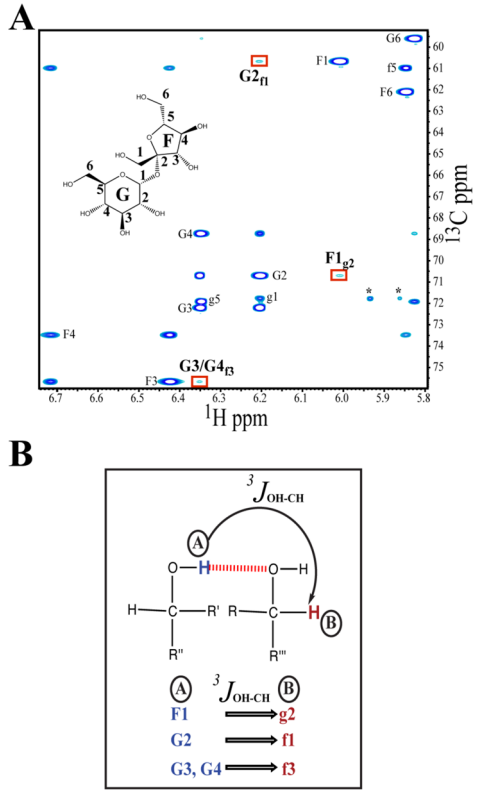

Figure 3. (A) Hydroxyl region of an HSQC-TOCSY spectrum tuned for hydrogen bond detection. Data were collected on a 300 mM sucrose sample, pH 6.5 at 268 K (700 MHz). Asterisks indicate ^{13}C decoupling artifacts. Atom assignments are as for Figure 2A. Correlations between hydroxyl protons and aliphatic protons are indicated with upper and lower case letters, respectively. Hydrogen bond peaks are indicated with red squares. Intraresidue correlations are not labeled. (B) Schematic representation of Hbonded pairs. Donor hydrogen is shown in blue; the hydrogen germinal to the acceptor hydroxyl group is shown in red. The $^{3}J_{OH-CH}$ that leads to observation of inter-residue cross peaks is depicted by arrows.

present results show that OHs can be detected and assigned without resorting to mixed solvents, supercooled temperatures, or extremely high concentrations (50 mM unlabeled sucrose can yield spectra with cross peaks' S/N ratio of at least ~10/1 in less than 4 h in a 500 MHz instrument using a conventional NMR probe). Structural information gathered from OHs under the conditions presented in this report, therefore, brings us closer to their function in a physiological context and minimizes the misinterpretation of data that would lead to virtual structures.

The hydroxyl hydrogens in a glucose−fructose inter-ring Hbond would link the otherwise isolated spin systems of glucose and fructose through the shared hydroxyl hydrogen. We therefore hypothesized that we could detect inter-ring hydrogen bonding (Hbonding) by observing inter-ring cross peaks in an HSQC-TOCSY experiment. With the OH assignments in hand, we were able to test this hypothesis. We probed the disaccharide for direct evidence of Hbonding, utilizing an HSQC-TOCSY experiment with longer τ_m (30 ms, instead of 10 ms). We observed inter-ring cross peaks between OH and CH from fructose and glucose (red squares, Figure 3A). Consequently, the two isolated spin systems (glucose and fructose) are connected through shared hydroxyl hydrogens. These inter-ring cross peaks indicate the presence of a $^{3}J_{OH-CH}$ coupling between the F1 hydroxyl proton and the g2 proton ($F1_{g2}$), $G2_{f1}$ and $G4_{f3}$ or $G3_{f3}$ (Figure 3A,B). Thus, inter-ring TOCSY transfer between OH and CH protons provides direct though-bond evidence of Hbonding in sucrose, via through-Hbond $^{3}J_{OH-CH}$ coupling.[43,44] Ongoing research in our groups is aimed at quantifying these coupling constant values.

Hbond donor/acceptor distinction (directionality) can be inferred from the same experiment: if a correlation is observed from a hydroxyl proton at carbon **A** of glucose to a carbon atom **B** of fructose (through ^{1}H at carbon **B**), it indicates that the hydroxyl proton at **A** is Hbonded to the oxygen atom at **B**. Conversely, if the correlation is observed from the hydroxyl signal of **B** to the carbon frequency of **A**, then the opposite is true. In the case of $F1_{g2}$, the OH proton of F1 is the donor and the oxygen atom at G2 is the acceptor (Figure 3B). For the $G2_{f1}$ cross peak, G2 OH is the donor and F1 the acceptor. Our results clearly show the presence of three Hbonds: $F1_{g2}$ and $G2_{f1}$, which involve the same hydroxyl groups that alternate between donor or acceptor of the Hbond; and between $G3_{f3}$ or $G4_{f3}$ ($G4/G3_{f3}$). The latter is ambiguous, as G4 and G3 hydroxyl proton resonances virtually overlap. The $G4_{f3}$ and $G3_{f3}$ Hbonds can potentially yield long-range cross peaks to adjacent OHs. These additional long-range correlations could afford resonance disambiguation. For instance, TOCSY transfer from G4 can yield long-range correlations to G3, g3, and g5 resonances (uppercase letters indicate hydroxyl ^{1}H resonances and lowercase letters aliphatic ^{1}H), whereas G3 can be coupled to G2, g2, G4, and g4. Therefore, a $G3_{f3}$ Hbond can also yield weaker $G4_{f3}$ and $G2_{f3}$ peaks. Conversely, $G4_{f3}$ Hbond can result in the observation of $G3_{f3}$ and $g5_{f3}$. The observation of $G2_{f3}$

dx.doi.org/10.1021/jp400402b | J. Phys. Chem. B 2013, 117, 4860−4869

(Figure S4 in the Supporting Information) and not a $g5_{f3}$ cross peak (not shown) in the HSQC-TOCSY spectra supports a $G3_{f3}$ Hbond (and not $G4_{f3}$). Additionally, the proton chemical shift of $G4/G3_{f3}$ cross peak appears to be that of G3. Therefore, we shall call this Hbond $G3_{f3}$ henceforth. However, the presence $G2_{f3}$ and absence of $g5_{f3}$ alone cannot rule out the existence of $G4_{f3}$ and/or $G3_{f3}$. Additional research is required to clarify this issue. Nonetheless, our results provide direct evidence that not only $F1_{g2}$ but also $G2_{f1}$ and $G3_{f3}$ Hbonds are present in solution.

While the intramolecular $F1_{g2}$ Hbond (Figure 3A) is supported by previous studies including MD simulations[45−47] as well as experimental data,[15,34,48−50] the $G3_{f3}$ hydrogen bond discovered in this study could, in principle, arise either inter- or intramolecularly. An intermolecular $G3_{f3}$ Hbond was reported in crystalline sucrose.[51] However, because the $G3_{f3}$ Hbond has not been reported in solution (directly or indirectly), we sought (1) to confirm the existence of Hbonds via a different experiment, since TOCSY could also yield ROESY artifacts, and (2) to determine whether the observed Hbonds are intra- or intermolecular.

To address the first point, we performed a selective COSY experiment that minimized water excitation (Figure 4). This experiment yielded the $G3_{f3}$ Hbond cross peak through a $^3J_{OH-CH}$ (Figure 4, red square). Interestingly, the selective COSY experiment also shows evidence for OH-to-OH correlations, as peaks proximal to the diagonal, in the 6−6.4 ppm region of the spectrum. A $^2J_{OH-OH}$ between G3−F3 is in agreement with the $G3_{f3}$ Hbond. Thus, while the HSQC-TOCSY experiment enables us to infer Hbonds through spin systems connection (inter-ring Hbonds via $^3J_{OH-CH}$), $^2J_{OH-OH}$ detected through COSY can potentially also report on intraring Hbonds.

Next, we establish whether the $G3_{f3}$ correlation arises from intra- or intermolecular Hbonds, by NMR and MD simulations. This distinction is important because while intramolecular Hbonds provide key structural details to establish glycan conformations, intermolecular Hbonds offer insight on how molecules interact.

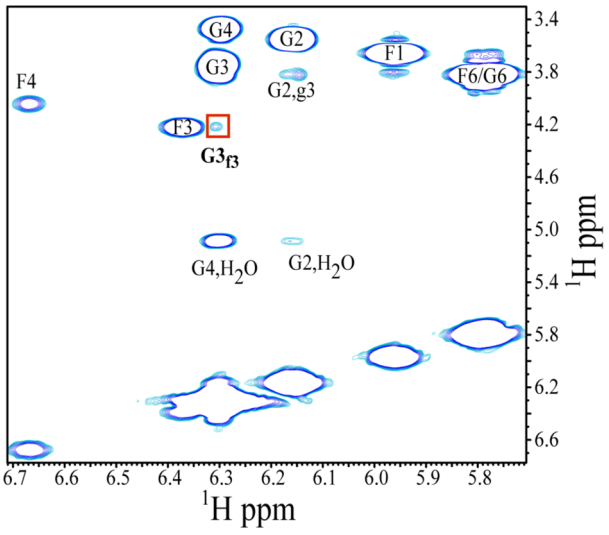

Figure 4. Region of a selective COSY spectrum collected under the same conditions as for Figure 3A. The $G3_{f3}$ Hbond-peak is indicated with a red square.

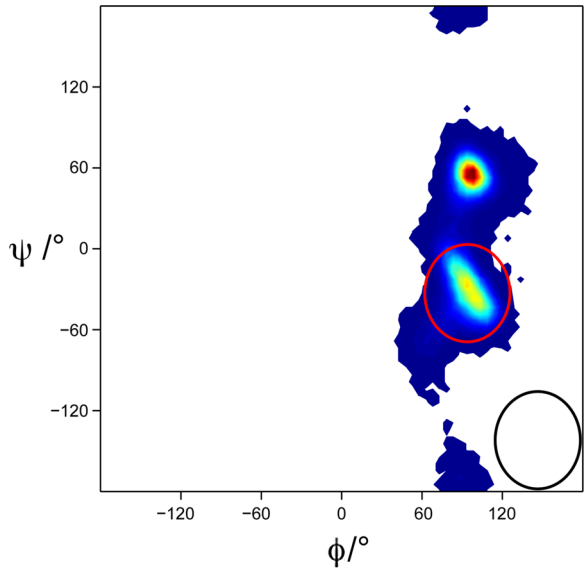

Figure 5. Population density distribution for the glycosidic torsion angles ϕ (O5g−C1g−O2f−C2f) and ψ (C1g−O2f−C2f−O5f) in sucrose from the simulation having c = 0.128 M. The population density is represented by colors, ranging from crimson (maximum population density) to dark blue (minimum population density). Ellipses depict glycosidic torsion angle values with maximum population density when the simulations are restrained with intramolecular Hbonds: $G3_{f3}$ (black) or $G4_{f3}$, respectively (red).

Unrestrained MD simulation results show that the conformational space available to sucrose in water is very similar to that presented by Xia and Case[46,52] as evidenced by the ϕ/ψ population distribution plot presented in Figure 5. Earlier molecular dynamics studies did not report any $G3_{f3}$ Hbonding, suggesting that a potential intramolecular accommodation of this bond would be in a relatively high-energy region of the conformational space, not likely to be sampled by regular molecular dynamics. In order to rapidly determine the plausibility of an intramolecular $G3_{f3}$ Hbond, we performed a Langevin dynamics simulation, restraining the G3 and F3 oxygen atom distance at 3.2 Å (conformations falling in the ϕ/ψ values depicted by a black ellipse in Figure 5). Similarly, restraining the G4 and F3 oxygen atom to a 3.2 Å distance did not yield a reasonable conformation either (red ellipse, Figure 5). In this latter case, although conformations obtained by restraining $G4_{f3}$ Hbond did satisfy favored dihedral angle values (Figure 5, red ellipse), the glucose ring geometry distorts in order to fit the Hbond restraint. The failure of these simulations to yield reasonable conformations satisfying the geometric criteria for a $G3_{f3}$ or $G4_{f3}$ Hbond suggests that it is not intramolecular. Taken together the unrestrained and restrained MD simulations lack an intramolecular $G3_{f3}$ or $G4_{f3}$ Hbond as a potential energy minimum, implying that this Hbond is intermolecular.

Based on ϕ/ψ values for the glycosidic torsions, 16 of the 20 published sucrose structures (Table S2 in the Supporting Information) agree with the MD-derived low-energy structures (and Case and co-workers' M1). Crystallographic ϕ or ψ values in sucrose structures are within 20° of the corresponding values found in our models. As expected, they also satisfy the oxygen−oxygen interatomic distance required for an Hbond between $G2_{f1}$ and $F1_{g2}$. However, because hydrogen atoms are absent in crystallographic models, Hbond directionality information may

dx.doi.org/10.1021/jp400402b | J. Phys. Chem. B 2013, 117, 4860−4869

be lost. In a crystal, a close O−O interatomic distance between F1 and G2 has been consistently observed.[48,49,51] Interestingly, the NMR results indicate the dynamic nature of sucrose's Hbonds in aqueous solution, as different Hbonded sucrose conformations, also called flip-flop Hbonds,[53] must coexist in solution to give rise to $G2_{f1}$ and $F1_{g2}$.

The sucrose structures that do not agree with our model were obtained by cocrystallizing the carbohydrate with its cognate protein. Among these proteins, one is involved in transport[54] and three chemically modify sucrose molecules.[55−58] It is plausible that a different sucrose structure is observed in the hydrolase or glycosyltransferase−sucrose complex, because sucrose conformation has to be optimal for the chemical modification to take place, and therefore a ground-state conformation may not be optimal for catalysis. Based on the surveyed structures, the other remaining sucrose conformations were cocrystallized with carrier proteins. From these remaining structures it becomes apparent that a ground-state structure is not required for transport purposes either.[54]

None of reported sucrose structures is consistent with an intramolecular $G3_{f3}$ Hbond.

In light of these results, we attempted to gain insight on sucrose aggregation via NMR. To this end, we explored Hbond cross peak dependence on sucrose concentration, at 263 K (Figure 6). Cross peak volume/intensity scaled linearly with sucrose concentration for the $F1_{g2}$, $G2_{f1}$ pair (R^2 = 0.99). The linear concentration dependence observed indicates that the $F1_{g2}$ and $G2_{f1}$ arise through intramolecular interactions. In contrast, the data obtained from the $G3_{f3}$ or $G4_{f3}$ correlation does not fit a straight line (R^2 = 0.88), but does fit a power equation (R^2 = 0.99) (Figure 6, black-filled squares), resulting in an essentially quadratic function. Nonlinear behavior is expected if aggregation occurs, indicating that the $G3_{f3}$ or $G4_{f3}$ cross peak arises from intermolecular contact, as predicted by MD simulations. This result is in agreement with the fact that a higher sucrose concentration is required for molecule−molecule interaction and for the observation of the $G3_{f3}$ or the $G4_{f3}$ cross peak (~400 mM for G4/$G3_{f3}$ versus ~200 mM for $F1_{g2}$ and $G2_{f1}$ Hbonds).

Equivalent experiments were performed in silico, where MD simulations were run at different sucrose concentrations, and the Hbonds were monitored throughout the trajectories. For the highest concentration (1.28 M), our results show that the $G3_{f3}$ Hbond is the second most prevalent intermolecular Hbond, second only to $F4_{g6}$. It should be noted that these HBonds are present to roughly the same extent, which at 1.28 M is 1.4% on a per-molecule basis, averaged over the trajectory. However, since the difference in occurrences in the MD simulations are not large enough, it is not possible to make the distinction between Hbonds that are observed, such as $G3_{f3}$, and those that are not, including the $G4_{f3}$ Hbond. The occurrence of the latter is 1.0% at 1.28 M. The concentration dependence of the presence of this Hbond is approximately quadratic, as expected for an intermolecular interaction. As can be seen in Figure 6, there is excellent agreement between the results obtained from MD simulations and NMR data providing evidence that while $F1_{g2}$ and $G2_{f1}$ are intramolecular Hbonds $G3_{f3}$ (or $G4_{f3}$) is intermolecular (Figure 7). The conformation at the glycosidic torsion angles did not differ significantly among the simulations at different concentrations of sucrose.

Furthermore, we explored the aggregation tendency of sucrose, by monitoring translational diffusion constants, via DOSY experiments, at 268 and 298 K (Figure 8). We expected

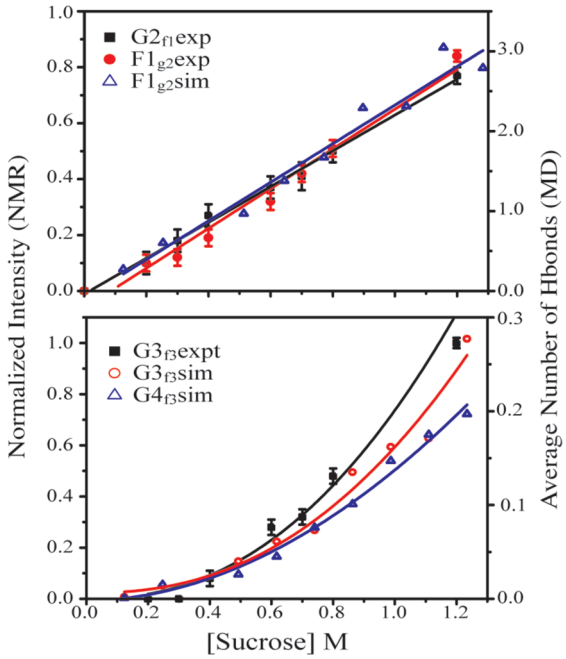

Figure 6. Peak intensity (NMR) and the average number of Hbonds during the MD simulation trajectories, as a function of sucrose concentration. Data was fitted to a linear equation, $y = ax + b$ (top) or to a power equation $y = ax^b$, that yielded b = 1.87 (bottom). Filled geometric symbols indicate experimental NMR data, whereas open symbols depict MD simulations data.

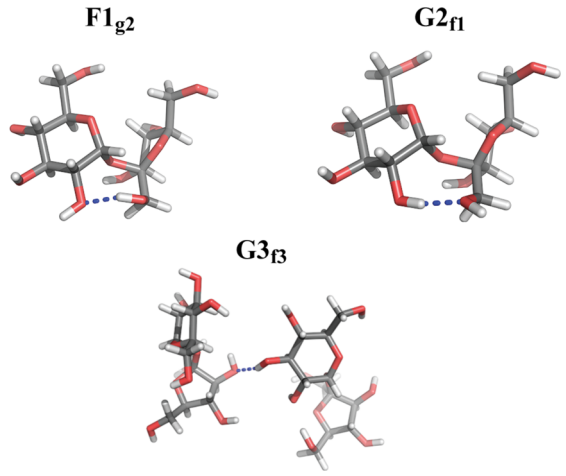

Figure 7. Sucrose 3D models depicting the three detected Hbonds (blue dash). Atoms are color coded as follows: hydrogen, white; oxygen, red; and carbon, gray.

a hydrodynamic radius increase as sucrose aggregates, thus affecting its translational diffusion. We used DSS as a hydrodynamic radius internal reference (and a negative control for aggregation). We report sucrose and trehalose diffusion constants relative to DSS translational diffusion.[59] We utilized trehalose as a positive control for aggregation. Trehalose is an excellent control: it has the same molecular weight as sucrose and was recently shown to aggregate even at 25 mM.[60] Diffusion constants measured at 500 μM for sucrose and trehalose at 298 K were used as reference diffusion for the monomeric states because they were considered to be at the infinite dilution limit, when the molecules are assumed to be monomers. At this concentration, the probability for encounter

dx.doi.org/10.1021/jp400402b | J. Phys. Chem. B 2013, 117, 4860−4869

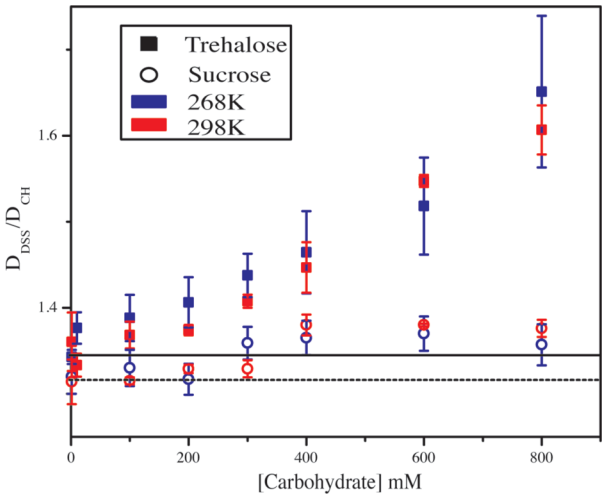

Figure 8. Diffusion of sucrose (○) and trehalose (■) relative to DSS measured at 268 K (blue) and 298 K (red). Dashed and solid lines indicate relative diffusion values at maximum dilution, for sucrose and trehalose, respectively. Diffusion rates are presented as relative to DSS diffusion to make the measurements independent of variations on sample viscosity and temperature.[59]

between solute molecules is very low (there are 112 000 molecules of water for every one of solute). If there is no aggregation, the relative diffusion should remain constant as a function of carbohydrate concentration. Figure 8 clearly shows that, for trehalose, the translational diffusion constant values deviates from the infinite dilution limit value (solid black line), reflecting aggregation at both temperatures, in agreement with the work presented by Halle and co-workers.[60] For sucrose, the changes are less evident; however, aggregation becomes apparent (deviations from the dashed line in Figure 8) at about 400 mM. If Hbonds only result from aggregation, then a change in the translational diffusion rate should correlate with the detection of Hbonds as carbohydrate's concentration increases. Interestingly, at about 400 mM we begin to detect the $G3_{f3}$ or $G4_{f3}$ Hbond (Figure 6). Thus, our diffusion experiments show that translational diffusion is not only a sufficiently sensitive to probe for aggregation in carbohydrates but also complements our results from Hbond concentration dependence study, together providing strong evidence that the $G3_{f3}$ Hbond results from intermolecular interaction/aggregation. Therefore, the $G3_{f3}$ Hbond reports on sucrose aggregation, which is detectable at ca. 400 mM in a 500 MHz instrument.

■ CONCLUDING REMARKS

In this report, we demonstrate the facile detection and unambiguous assignment of hydroxyl hydrogen atoms in a wide range of temperatures (263−283 K for sucrose and up to 298 K for trehalose). Facile detection of OHs provides a previously unavailable structural probe, without the requirement of ^{13}C labeling. This finding is significant because one can envision the use of these resonances as handles to facilitate assignment and to obtain inter-residue NOEs/ROEs, which are generally sparse in solution NMR of glycans. Additionally, OH participating in Hbonds can be utilized to extract through-Hbond coupling constants.[43,44,61] Characterization of Hbonds through accurately determining through-Hbond coupling constants is an important next step. To this end, ideally, direct $^2J_{OH\text{-}C}$ correlations, such as the ones provided by HSQC/HMQC/HMBC experiments, would facilitate their measurement. However, OH exchange with the solvent reduces direct magnetization transfer between OH and ^{13}C. Nonetheless, observation of hydroxyl signals and related Hbonds constitutes an essential first step to accomplish this goal.

We showed that with the unambiguous assignment of hydroxyl proton resonances we could detect Hbonds, which are known to provide valuable structural information for other biomolecules. Detection of intra- or intermolecular Hbonds in solution is of great significance for structural glycobiology. On one hand, detection of intramolecular Hbonds can increase our understanding of forces that dictate glycan structure, because only certain conformations will permit the correct orientation of donor and acceptor atoms. On the other hand, detection of intermolecular Hbonds will aid in the understanding of glycan−glycan interactions, which may in turn modulate protein−glycan recognition through the formation of patches on cell surfaces. Although the strategy described herein has immediate applicability to samples in more defined solvents, as the ones described in this report, one can envision its applicability to more complex samples such as biological fluids. However, to reach this goal, labeled compounds are mandatory. Labeled samples will serve a 2-fold purpose: they will increase the sensitivity and they will enable data acquisition free of background, which otherwise would be overwhelming for a biological milieu. Scientific efforts in our laboratories are focusing on this direction; however, further research is needed to achieve this goal.

Glycan solution structure determination should have broad impact from drug design and vaccine development to material science. Additionally, crystallographic studies of glycans are rare as crystals are difficult to obtain; therefore, solution NMR is a valuable complementary tool that can contribute to establishing structure−function relationships for glycans in order to decipher the "carbohydrate code".[62] Interestingly, the importance of transient structures in intrinsically disordered systems is becoming more apparent,[63] and with it, the need for new ways to detect and characterize these structures becomes essential. The present report provides a new strategy to observe, in a wide range of temperatures, previously unavailable structural probes that can uncover structural elements in intrinsically flexible systems. Hydroxyl proton detection can not only lead to the observation of Hbonds, and to infer their directionality, as we have shown, but could also provide yet unexplored NOEs/ROEs and catalyze the discovery of secondary structural patterns in glycans. Additionally, our discovery can impact the study of other biomolecules such as protein and nucleic acids, which contain exchangeable protons (e.g., OH and SH) that can be detected to discern structural or catalytic roles through their observation with the herein presented methodology. Moreover, detection of intermolecular Hbonds can be envisioned as a first step to begin to understand carbohydrate−carbohydrate complexes and their role in biological systems.

■ ASSOCIATED CONTENT

Supporting Information

Supplementary figures and tables referenced in the text. This material is available free of charge via the Internet at http://pubs.acs.org.

dx.doi.org/10.1021/jp400402b | J. Phys. Chem. B 2013, 117, 4860−4869

AUTHOR INFORMATION

Corresponding Author

*E-mail: daron.freedberg@fda.hhs.gov.

Author Contributions

The manuscript was written through contributions of all authors. All authors have given approval to the final version of the manuscript.

Notes

The authors declare no competing financial interest.

ACKNOWLEDGMENTS

We gratefully acknowledge helpful discussions with Drs. Dennis A. Torchia, Hugo Azurmendi, and Bingwu Yu. This work was supported by intramural funds from CBER/FDA (M.D.B. and D.I.F.) and a grant from the Swedish Research Council (R.P. and G.W.). Computing resources were kindly provided by the Center for Parallel Computers (PDC), Stockholm, Sweden.

ABBREVIATIONS

COSY, correlation spectroscopy; F, fructose; G, glucose; Hbond, hydrogen bond; MD, molecular dynamics; SW, spectral window; HSQC, heteronuclear single quantum coherence; OH, hydroxyl group; TOCSY, total correlation spectroscopy; τ_m, mixing time

REFERENCES

(1) Apweiler, R. H., H.; Sharon, N. *Biochim. Biophys. Acta* **1999**, *1473*, 4.
(2) Bialas, N.; Kasperkiewicz, K.; Radziejewska-Lebrecht, J.; Skurnik, M. *Arch. Immunol. Ther. Ex.* **2012**, *60*, 199.
(3) Jodar, L.; Feavers, I. M.; Salisbury, D.; Granoff, D. M. *Lancet* **2002**, *359*, 1499.
(4) Garcia-Ojeda, P. A.; Hardy, S.; Kozlowski, S.; Stein, K. E.; Feavers, I. M. *Infect. Immun.* **2004**, *72*, 3451.
(5) Rutishauser, U.; Landmesser, L. *Trends Neurosci.* **1996**, *19*, 422.
(6) Karlsson, K.-A. *Curr. Opin. Struct. Biol.* **1995**, *5*, 622.
(7) Collin, J. G. M. *J. Innate Immun.* **2012**, *4*, 121.
(8) Helenius, A.; Aebi, M. *Science* **2001**, *291*, 2364.
(9) Rasmussen, J. R. *Curr. Opin. Struct. Biol.* **1992**, *2*, 682.
(10) Walt, D.; Aoki-Kinoshita, K. F.; Bertozzi, C.; Boons, G.-J.; Darvill, A.; Hart, G.; Kiessling, L.; Lowe, J.; Moon, R. J.; Paulson, J. C.; Sasisekharan, R.; Varki, A. P.; Wong, C.-H. *Transforming Glycoscience: A Roadmap for the Future*; The National Academies Press: Washington, DC, 2012.
(11) Vinogradov, E.; Bock, K. *Angew. Chem.* **1999**, *38*, 671.
(12) Bubb, W. A. *Concepts Magn. Reson. A* **2003**, *19*, 1.
(13) Battistel, M. D.; Shangold, M.; Trinh, L.; Shiloach, J.; Freedberg, D. I. *J. Am. Chem. Soc.* **2012**, *134*, 10717.
(14) Norris, S. E.; Landström, J.; Weintraub, A.; Bull, T. E.; Widmalm, G.; Freedberg, D. I. *Biopolymers* **2012**, *97*, 145.
(15) Sheng, S. Q.; van Halbeek, H. *Biochem. Biophys. Res. Commun.* **1995**, *215*, 504.
(16) van Halbeek, H. *Curr. Opin. Struct. Biol.* **1994**, *4*, 697.
(17) Poppe, L.; van Halbeek, H. *Nat. Struct. Biol.* **1994**, *1*, 215.
(18) Batta, G.; Kövér, K. E. *Carbohydr. Res.* **1999**, *320*, 267.
(19) Fierman, M.; Nelson, A.; Khan, S. I.; Barfield, M.; O'Leary, D. J. *Org. Lett.* **2000**, *2*, 2077.
(20) Symons, M. C. R.; Benbow, J. A.; Harvey, J. M. *Carbohydr. Res.* **1980**, *83*, 9.
(21) Craig, B. N.; Janssen, M. U.; Wickersham, B. M.; Rabb, D. M.; Chang, P. S.; O'Leary, D. J. *J. Org. Chem.* **1996**, *61*, 9610.
(22) Vasquez, T. E.; Bergset, J. M.; Fierman, M. B.; Nelson, A.; Roth, J.; Khan, S. I.; O'Leary, D. J. *J. Am. Chem. Soc.* **2002**, *124*, 2931.
(23) Delaglio, F.; Grzesiek, S.; Vuister, G., W.; Zhu, G.; Pfeifer, J.; Bax, A. *J. Biomol. NMR* **1995**, *6*, 277.
(24) Vranken, W. F.; Boucher, W.; Stevens, T. J.; Fogh, R. H.; Pajon, A.; Llinás, P.; Ulrich, E. L.; Markley, J. L.; Ionides, J.; Laue, E. D. *Proteins* **2005**, *59*, 687.
(25) Piotto, M.; Saudek, V.; Sklenář, V. *J. Biomol. NMR* **1992**, *2*, 661.
(26) Bax, A.; Ikura, M.; Kay, L. E.; Torchia, D. A.; Tschudin, R. *J. Magn. Reson.* **1990**, *86*, 304.
(27) Aue, W. P.; Bartholdi, E.; Ernst, E. E. *J. Chem. Phys.* **1976**, *64*, 2229.
(28) Hahn, E. L. *Phys. Rev.* **1950**, *77*, 297.
(29) Hahn, E. L. *Phys. Rev.* **1950**, *80*, 580.
(30) Antalek, B.; Windig, W. *J. Am. Chem. Soc.* **1996**, *118*, 10331.
(31) Brooks, B. R.; Brooks, C. L.; MacKerell, A. D., Jr.; Nilsson, L.; Petrella, R. J.; Roux, B.; Won, Y.; Archontis, G.; Bartels, C.; Boresch, S.; Caflisch, A.; Caves, L.; Cui, Q.; Dinner, A. R.; Feig, M.; Fischer, S.; Gao, J.; Hodoscek, M.; Im, W.; Kuczera, K.; Lazaridis, T.; Ma, J.; Ovchinnikov, V.; Paci, E.; Pastor, R. W.; Post, C. B.; Pu, J. Z.; Schaefer, M.; Tidor, B.; Venable, R. M.; Woodcock, H. L.; Wu, X.; Yang, W.; York, D. M.; Karplus, M. *J. Comput. Chem.* **2009**, *30*, 1545.
(32) Raman, E. P.; Guvench, O.; MacKerell, A. D., Jr. *J. Phys. Chem. B* **2010**, *114*, 12981.
(33) Widmalm, G.; Pastor, R. W. *J. Chem. Soc., Faraday Trans.* **1992**, *88*, 1747.
(34) Brown, G. M.; Levy, H. A. *Acta Crystallogr. Sect. B: Struct. Commun.* **1973**, *B29*, 790.
(35) Jorgensen, W. L.; Chandrasekhar, J.; Madura, J., D.; Impey, R. W.; Klein, M. K. *J. Chem. Phys.* **1983**, *79*, 926.
(36) Feller, S. E.; Zhang, Y.; Pastor, R. W.; Brooks, B. R. *J. Chem. Phys.* **1995**, *103*, 4613.
(37) Chirife, J. B.; M., P. *J. Food Eng.* **1997**, *33*, 221.
(38) Williamson, R. T.; Marquez, B. L.; Gerwick, W. H.; Kover, K. E. *Magn. Reson. Chem.* **2000**, *38*, 265.
(39) Bax, A. *Isr. J. Chem.* **1988**, *28*, 309.
(40) Sandström, C.; Baumann, H.; Kenne, L. *J. Chem. Soc., Perkin Trans. 2* **1998**, 809.
(41) St-Jacques, M.; Sundararajan, P. R.; Taylor, K. J.; Marchessault, R. H. *J. Am. Chem. Soc.* **1976**, 4386.
(42) Xia, J.; Case, D. A. *Biopolymers* **2012**, *97*, 289.
(43) Dingley, A. J.; Grzesiek, S. *J. Am. Chem. Soc.* **1998**, *120*, 8293.
(44) Cordier, F.; Grzesiek, S. *J. Am. Chem. Soc.* **1999**, *121*, 1601.
(45) Immel, S.; Lichtenthaler, F. W. *Liebigs Ann.* **1995**, 1925.
(46) Xia, J.; Case, D. A. *Biopolymers* **2012**, *97*, 276.
(47) Bagley, S.; Odelius, M.; Laaksonen, A.; Widmalm, G. *Acta Chem. Scand.* **1994**, *48*, 792.
(48) Brown, G. M.; Levy, H. A. *Science* **1963**, *141*, 921.
(49) Hanson, J. C.; Sieker, L. C.; Jensen, L. H. *Acta Crystallogr. Sect. B: Struct. Commun.* **1973**, *B 29*, 797.
(50) Bock, K.; Lemieux, R. U. *Carbohydr. Res.* **1982**, *100*, 63.
(51) Patyk, E.; Skumiel, J.; Podsiadlo, M.; Katrusiak, A. *Angew. Chem., Int. Ed.* **2012**, *51*, 2146.
(52) Nagae, M.; Yamaguchi, Y. *Int. J. Mol. Sci.* **2012**, *13*, 8398.
(53) Olschewski, M.; Lindner, J.; Vöhringer, P. *Angew. Chem., Int. Ed.* **2013**, *52*, 2602.
(54) Forst, D.; Welte, W.; Wacker, T.; Diederichs, K. *Nat. Struct. Mol. Biol.* **1998**, *5*, 37.
(55) Berman, H. M.; Westbrook, J.; Feng, Z.; Gilliland, G.; Bhat, T. N.; Weissig, H.; Shindyalov, I. N.; Bourne, P. E. *Nucleic Acids Res.* **2000**, *28*, 235.
(56) Mirza, O.; Skov, L. K.; Remaud-Simeon, M.; Potocki de Montalk, G.; Albenne, C.; Monsan, P.; Gajhede, M. *Biochemistry* **2001**, *40*, 9032.
(57) Skov, L. K.; Mirza, O.; Sprogoe, D.; Dar, I.; Remaud-Simeon, M.; Albenne, C.; Monsan, P.; Gajhede, M. *J. Biol. Chem.* **2002**, *277*, 47741.
(58) Meng, G. Y.; Futterer, K. *Nat. Struct. Biol.* **2003**, *10*, 935.
(59) Macchioni, A.; Ciancaleoni, G.; Zuccaccia, C.; Zuccaccia, D. *Chem. Soc. Rev.* **2008**, *37*, 479.
(60) Winther, L. R.; Qvist, J.; Halle, B. *J. Phys. Chem. B* **2012**, *116*, 9196.

(61) Barfield, M.; Bergset, J. M.; O'Leary, D. J. *Magn. Reson. Chem.* **2001**, *39*, S115.
(62) Laine, R. A. *Pure Appl. Chem.* **1997**, *69*, 1867.
(63) Lee, S.-H.; Kim, D.-H.; Han, J. J.; Cha, E.-J.; Lim, J.-E.; Cho, Y.-J.; Lee, C.; Han, K.-H. *Curr. Protein Pept. Sci.* **2012**, *13*, 34.